ISSN 1063-7834, Physics of the Solid State, 2018, Vol. 60, No. 9, pp. 1768–1777. © Pleiades Publishing, Ltd., 2018.
Original Russian Text © A.V. Trukhanov, V.G. Kostishin, V.V. Korovushkin, L.V. Panina, S.V. Trukhanov, V.A. Turchenko, I.S. Polyakov, R.Kh. Rakhmatullin, G.A. Filatov, T.I. Zubar', V.V. Oleinik, E.S. Yakovenko, L.Yu. Matsui, L.L. Vovchenko, V.L. Launets, E.L. Trukhanova, 2018, published in Fizika Tverdogo Tela, 2018, Vol. 60, No. 9, pp. 1723–1732.

MAGNETISM

Mössbauer Studies and the Microwave Properties of Al^{3+}- and In^{3+}-Substituted Barium Hexaferrites

A. V. Trukhanov[a, b, *], V. G. Kostishin[b], V. V. Korovushkin[b], L. V. Panina[b], S. V. Trukhanov[a], V. A. Turchenko[c], I. S. Polyakov[b], R. Kh. Rakhmatullin[b], G. A. Filatov[b], T. I. Zubar'[d], V. V. Oleinik[e], E. S. Yakovenko[e], L. Yu. Matsui[e], L. L. Vovchenko[e], V. L. Launets[e], and E. L. Trukhanova[a, b]

[a] *Scientific and Practical Materials Research Centre, National Academy of Sciences of Belarus, Minsk, 220072 Belarus*
[b] *National University of Science and Technology MISiS, Moscow, 119049 Russia*
[c] *Frank Neutron Physics Laboratory, Joint Nuclear Research Institute, Dubna, Moscow oblast, 141980 Russia*
[d] *A.V. Lykov Heat and Mass Transfer Institute of National Academy of Sciences of Belarus, Minsk, 220072 Belarus*
[e] *Taras Shevchenko National University of Kyiv, Kyiv, 01033 Ukraine*
**e-mail: truhanov86@mail.ru*

Received March 27, 2018

Abstract—The correlation of the chemical composition, the structure, and the microwave characteristic of solid solutions of the $BaFe_{12-x}D_xO_{19}$ ($0.1 \le x \le 1.2$) barium hexaferrite substituted with diamagnetic Al^{3+} and In^{3+} ions has been studied. The precise data on the crystal structure have been obtained by powder neutron diffraction using a high-resolution Fourier diffractometer (Dubna, JINR). The data on the distribution of the diamagnetic substituting ions in the hexaferrite structure have been obtained by Mössbauer spectroscopy. The microwave properties (the transmittance and the reflectance) have been studied in the frequency range 20–65 GHz and in external magnetic fields to 8 kOe. It is found that the transmission spectra are characterized by a peak that corresponds to the resonant frequency of the electromagnetic energy absorption, which is due to the ferromagnetic resonance phenomenon. The correlation of the chemical composition, the features of the ion distribution in the structure, and the electromagnetic properties has been revealed. It is shown that external magnetic fields shift the absorption peak of electromagnetic radiation to higher frequencies due to an increase in the magnetocrystal anisotropy. The results enable the conclusion that the features of the intrasublattice interactions and the electromagnetic properties should be explained using the phenomenological Goodenough–Kanamori model.

DOI: 10.1134/S1063783418090342

1. INTRODUCTION

M-type hexagonal ferrite and their solid solutions have a crystal structure of magnitoplumbite $PbFe_{12}O_{19}$ that was studied in [1] for the first time in 1938. As a rule, it is well described in terms of space group $P6_3/mmx$ (no. 194) with the hexagonal unit cell $a = b \approx 5.90$ Å, $c \approx 23.30$ Å containing two molecules per the formula unit. Iron ions are distributed in five nonequivalent crystallographic positions (anion environments): octahedral $2a$, $4f_2$, and $12k$, bipyramidal $2b$, and tetragedral $4f_1$ oxygen environments. These compounds are characterized by the coexistence of strong intrasublattice Heisenberg exchange interaction and a weak competition of intersublattice exchange interactions [2]. The intrasublattice interactions, as a rule, dominate and form a collinear ferromagnetic structure with high energies of the exchange interactions. A strong correlation of the intrasublattice exchange interactions and an attenuation of the intersublattice exchange can lead to the formation of noncollinear atypical magnetic structures (conical and helicoidal magnetic structures, etc.).

Hexagonal barium ferrite $BaFe_{12}O_{19}$ (or BFO) and $BaFe_{12-x}D_xO_{19}$ (or BFDO) solid solutions based on it (with isovalent or heterovalent diamagnetic substitution for Fe^{3+} in the B sublattice) attract a great attention of researchers [3–8] due to their excellent functional properties [9]. Their chemical inertness and corrosion resistance [10] make them ecologically safe and stable. The coexistence of a giant coercive force, high residual magnetization, and high electrical resistance make these materials suitable for application in practice. Until recently, BFO and BFDO were widely used as permanent magnets [11]. Even at the present time more than 80% commercial permanent magnets in the world are hexagonal ferrites. Hexaferrites were also considered promising materials for magnetic recording devices (perpendicular type of magnetiza-

tion) [12]. Recently, the number of publications on BFO and BFDO caused by their mutiferroic properties (coexistence of the ferromagnetic and ferroelectric orderings) has increased significantly [13–18]. A high electrical resistance of these materials makes it possible to use them for high-frequency applications (as elements of functional devices of microwave equipment and electromagnetic radiation (EMR) absorbers) [21–24].

The development of mobile communication, the internet, and digital networks need the increase in the velocity and volume of data transmission which are possible in going from the centimeter wavelengths to the millimeter range corresponding to frequencies of 30–100 GHz. The M-type hexaferrites have high fields of the magnetic crystallographic anisotropy and capable of operating in this range. These materials are promising for developing and designing functional devices of microwave electronics: isolators, circulators, phase-shifters, elements of reception–transmission antennas, and also efficient EMR absorbers to provide the electromagnetic compatibility [25–30]. Doping or replacing barium hexaferrite with various diamagnetic ions leads to a significant changes in the magnetic characteristics and, as a result, to a change in the operating frequency range.

BFO-based compounds are promising materials for the absorption (attenuation) of electromagnetic radiation (EMR) with the allowance for their magnetic properties and the possibilities of their modifications. To improve the magnetic and functional properties of $BaFe_{12}O_{19}$, iron ions are usually replaced with isovalent diamagnetic ions D^{3+} (isovalent substitution) [31–34] or heterovalent diamagnetic D^{4+} or D^{2+} ions (heterovalent substitution). The diamagnetic substitution in BFO changes the features of the crystal structure (unit cell distortion, microdeformations, and changes in the Fe–O bond length) and the magnetic structure (attenuation of the magnetic exchange interaction and the magnetic structure frustration). The modification of the crystal and magnetic structures must change the electromagnetic characteristics. It is known that the selective EMR absorption in complex magnetic oxides is realized by the two main mechanisms: the domain boundary resonance and the natural ferromagnetic resonance (NFMR) (the precession frequency of the magnetization vector) [35, 36]. The main contribution to the high-frequency absorption is exactly related to NFMR.

The working range of BFO is determined by the frequency range in which the permeability (the imaginary part) is effectively changed, which takes place near NFMR. The application of hexagonal ferrites with a high degree of the crystal and magnetic anisotropies allow one frequency-selective control the SMR characteristics by shifting the NFMR resonant frequency. The NFMR frequency of nonsubstituted $BaFe_{12}O_{19}$ is in the range 49–50 GHz and is dependent on the value of the internal magnetic anisotropy field H_a:

$$\omega = \gamma H_a, \quad (1)$$

ω is the NFMR frequency and γ is the giromagnetic ratio.

The NFMR region in polycrystalline ferrites is sufficiently wide and it can be controlled varying the value of H_a, for example, by introducing various diamagnetic ions in the ferrite structure and also using an external magnetic field H_0:

$$f = \gamma(H_0 + H_a - 4\pi M_s), \quad (2)$$

$4\pi M_s$ is the demagnetization factor.

Thus, we can change amplitude–frequency characteristics of the resonance controlling the content of substituting ions.

In this work, we studied the correlation between the concentration of diamagnetic ions (Al^{3+}, In^{3+}) and the electromagnetic properties of solid solutions of the $BaFe_{12-x}D_xO_{19}$ barium hexaferrite (D = Al^{3+} and In^{3+}; $0 \le x \le 1.2$). The diamagnetic ions (Al^{3+} and In^{3+}) were chosen by two reasons: (i) the difference in the ionic radii: $r_{Al}^{3+} = 0.54$ Å $\ll r_{Fe}^{3+} = 0.64$ Å $< r_{In}^{3+} = 0.94$ Å; (ii) the different electronic ion structures. Aluminum ion has a completely occupied *p*-shell and empty *d*-shell and can called "d^0-ion." The Al^{3+} electronic structure $2s^22p^6$ corresponds to the configuration of noble gas Ne. Indium ion has the completely occupied *d*-shell and the empty *s*-shell and can be called "d^{10}-ion" or "completely occupied ion." The electronic structure of In^{3+}–$4d^{10}5s^0$ corresponds to the electronic configuration of noble Pd metal. The main aim of this work is to study the correlation of the chemical composition, the structure, and the microwave characteristics of solid solutions of the $BaFe_{12-x}D_xO_{19}$ ($0.1 \le x \le 1.2$) barium hexaferrite substituted with Al^{3+} and In^{3+} ions.

2. EXPERIMENTAL

The ceramic $BaFe_{12-x}D_xO_{19}$ samples (D = Al^{3+} and In^{3+}, $0.1 \le x \le 1.2$) were prepared of oxides Fe_2O_3 and D_2O_3 (D = Al^{3+} and In^{3+}) and carbonate $BaCO_3$ using the two-stage reaction (the common solid reaction method). All the initial reagents were high purity. The oxides and the carbonate were mixed in an exactly stoichiometric proportion. The preliminary synthesis was performed at 1200°C in air for 6 h. The final synthesis was carried out at 1300°C in air for 6 h. After the synthesis, the samples were slowly cooled (100°C h^{-1})

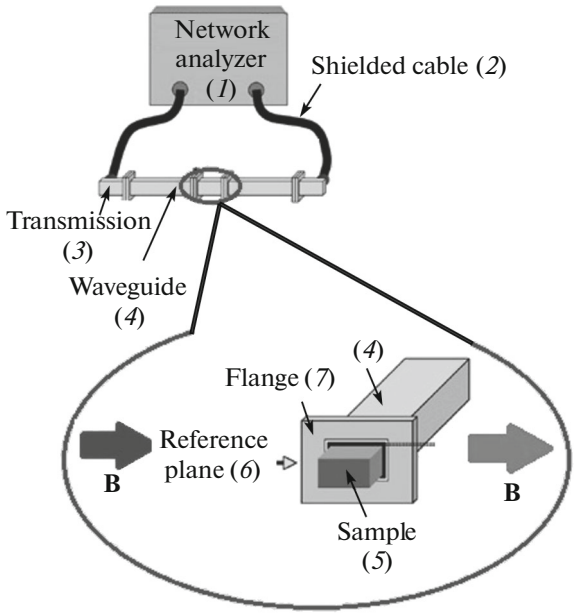

Fig. 1. Schematic of the method of measurements of the electromagnetic characteristics by waveguide method (*1* is the network vector analyzer, *2* is the shielded cable, *3* is the output for measuring the transmission spectra, *4* is the waveguide, *5* is the sample, *6* is the reference plane, and *7* is the flange).

[37]. The synthesis of the $BaFe_{12-x}D_xO_{19}$ samples can be represented by the following reaction:

$$BaCO_3 + \left(6 - \frac{1}{2}x\right)Fe_2O_3 + \left(\frac{1}{2}x\right)D_2O_3 \rightarrow BaFe_{12-x}D_xO_{19} + CO_2\uparrow. \quad (3)$$

The unit cell parameters (*a*, *c*, and *V*) were calculated based on the experimental neutron diffraction data. The neutron diffraction studies were carried out with the high-resolution Fourier diffractometer (HRFD). HRFD is a time-of-flight diffractometer at the IBR-2M pulsed reactor in Dubna with a relative large (~21.131 m) path length from the moderator to the detector and it has the extremely high resolution ($\delta d/d \approx 0.001$) that, in addition, is not almost dependent on the interplanar spacing in a wide range d_{hkl}. The high-resolution neutron diffraction patterns were measured by detectors disposed at average scattering angle of ±152° in the interplanar spacing from 0.6 to 3.6 Å. The experimental flight-of-time neutron diffraction patterns were carried out by the FullProfile Rietveld [38] using the MRIA and FullProf program packages [39] and built-in tables for coherent scattering length and magnetic form-factors. The distribution of the substituting ions in the hexaferrite structure was studied by Mössbauer spectroscopy using a Ms1104-Em spectrometer. The data processing was carried out using the UnivemMs software. The electromagnetic properties were measured by the waveguide method (Fig. 1) using an Agilent network analyzer.

The studies were performed in the range 20–65 GHz. Transmittances k_{tr} and reflectances k_{ref} were determined as

$$k_{tr} = 10\log\left(\frac{P_{tr}}{P_{inc}}\right) \quad \text{and} \quad k_{ref} = 10\log\left(\frac{P_{ref}}{P_{inc}}\right), \quad (4)$$

where P_{inc} is the initial (incident) EMR power, P_{tr} is the EMR power transmitting through the sample, P_{ref} is the reflected EMR power. The EMR absorption coefficient k_{abs} can be calculated using coefficients k_{tr} and k_{ref} obtained experimentally taking into account the energy conservation law by formula

$$k_{abs} = 10\log(1 - 10^{0.1k_{tr}} - 10^{0.1k_{ref}}). \quad (5)$$

3. EXPERIMENTAL RESULTS AND DISCUSSION

According to the neutron diffraction data, all the $BaFe_{12-x}D_xO_{19}$ samples ($D = Al^{3+}$ and In^{3+}, $0.1 \le x \le 1.2$) are characterized by the hexagonal structure with space group $P6_3/mmc$ with two molecules in the unit cell ($Z = 2$) (Fig. 2). It was stated that all the samples are single-phase. The correspondence factors obtained as a result of processing the neutron diffraction spectra (R_{wp}, R_{exp}, R_B, R_{Mag}, and χ^2) suggest that the study samples are characterized by high quality, and the level of the experimental data processing is relevant. Figure 2 shows the structure formula model (the right picture) and the concentration dependences of the unit cell parameters (*a*, *c*, and *V*) for $BaFe_{12-x}Al_xO_{19}$ (Fig. 2a) and $BaFe_{12-x}In_xO_{19}$ (Fig. 2b).

The unit cell volume of the Al-substituted hexaferrites is smaller than that of nonsubstituted $BaFe_{12}O_{19}$. The unit cell parameters and volume decreased, while the aluminum concentration increased from 0.1 to 1.2 (Fig. 2a). The monotonic decrease of the volume from 696.91 Å^3 to 690.12 Å^3 is explained by insignificant decrease in parameters *a* (from 5.889 to 5.870 Å) and *c* (from 23.172 to 23.126 Å) in the range $0.1 \le x \le 1.2$. The reason of this dependence is a smaller Al^{3+} ion radius (0.540 Å) as compared to the Fe^{3+} ion radius (0.640 Å). The situation is opposite in the case of the In-substituted samples. Whereas the In^{3+} concentration increases, the unit cell parameters increase too (Fig. 2b). The nearly linear increase in the volume from 698.82 Å^3 to 714.63 Å^3 is due to a significant increase in parameters *a* (from 5.85 to 5.932 Å) and *c* (from 23.217 to 23.445 Å) in the range $0.1 \le x \le 1.2$. We can state that it is a result of substituting of In^{3+} ion with larger ionic radius (0.940 Å) for iron ion.

To determine the character of the distribution of substituting ions in the hexaferrite structure and to study the influence of the positions occupied with dia-

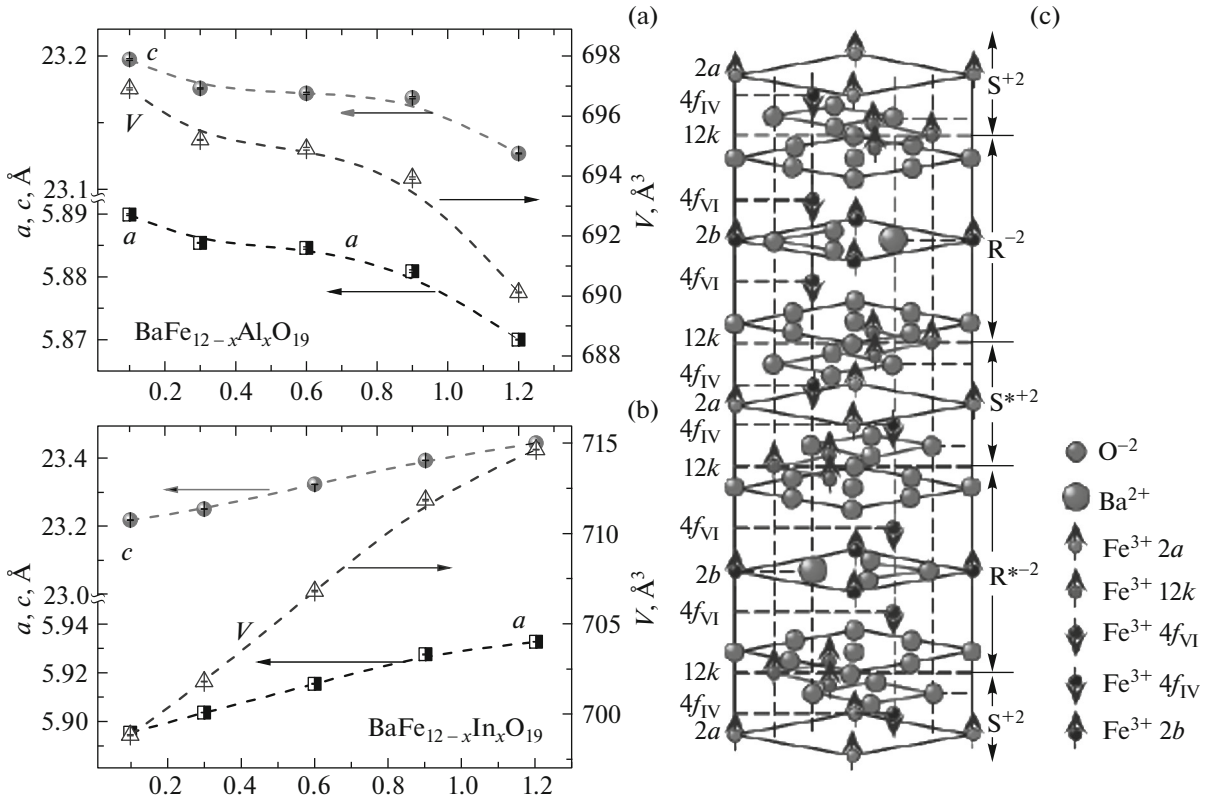

Fig. 2. Model of the barium hexaferrite structural formula (the right picture) and the concentration dependences of the unit cell parameters (a, c, and V) for $BaFe_{12-x}Al_xO_{19}$ (a) and $BaFe_{12-x}In_xO_{19}$ (b).

magnetic ions on the exchange interaction intensity we used Mössbauer spectroscopy. Figure 3 shows the Mössbauer spectra of $BaFe_{12-x}Al_xO_{19}$ (Fig. 3a) and $BaFe_{12-x}In_xO_{19}$ (Fig. 3b), where $x = 0.1$ and 1.2. The features of the Mössbauer parameters are given in Table 1. The nonsubstituted BFO ($x = 0$) has five sextets, according to the Fe^{3+} positions (oxygen coordinations): octahedral 12k, 4f_2, and 2a, tetrahedral 4f_1, and bipyramidal 2b. The magnetic fields at ^{57}Fe nuclei are different for all the positions and are in the following order: $B_{eff}Fe(4f_2) > B_{eff}Fe(2a) > B_{eff}Fe(4f_1) > B_{eff}Fe(12k) > B_{eff}Fe(2b)$.

All the BFDO samples with $x = 0.1$ demonstrate the appearance of a new sixth sextet. The appearance of additional new sextets denoted as 12k^1 corresponds to a distorted type of the 12k sublattice. We assume that diamagnetic cations at low concentrations are distributed in the 2b position, which lead to a weakening of the exchange couplings Fe^{3+} (2b)–O–Fe^{3+} (12k) and Fe^{3+} (2b)–O–Fe^{3+} (2a) (due to the magnetic structure frustration at a weakening of the long-range order of the exchange interactions). As a result, the nonequivalent positions of Fe^{3+} (for the 12k positions) with a lower field (B_{eff}) in ^{57}Fe nuclei. This corresponds to sextet C6 in the spectra for Fe^{3+} (12k^1).

In theory, the 12k^1 state can forms as a result of the distribution of cations D^{3+} in the 12k position, since it builds triads, but the total area of the sextet for C1 (12k) and C6 (12k^1) does not confirm this assumption. At the same time, the area of the sextet corresponding to the 4f_1 increases. The increase in this sextet area can be the result of the superposition with the 2a sextet. The distribution of cations in the 2b position, as aforementioned, leads to the attenuation of the exchange interactions inside the Fe^{3+} (2b)–O–Fe^{3+} (2a), which leads to the nonequivalent state of Fe^{3+} for the 2a position with a lower effective field at ^{57}Fe nuclei and with the parameters analogous to position 4f_1. A partial agreement of overlapping sextets confirms the increase in the Fe^{3+} (4f_1) line width. The fields (B_{eff}) at ^{57}Fe nuclei in the samples with a low substitution ($x = 0.1$) are analogous to the fields in the nonsubstituted hexaferrite as one new value of B_{eff} for 12k^1. Thus, the field in ^{57}Fe at $x = 0.1$ has the following order: $B_{eff}Fe(4f_2) > B_{eff}Fe(2a) > B_{eff}Fe(4f_1) > B_{eff}Fe(12k) > B_{eff}Fe(2b) > B_{eff}Fe(12k^1)$.

However, a completely different situation is observed for concentration $x = 1.2$. All the substituted BFO samples with $x = 1.2$ demonstrated the appearance of the seventh sextet. We assumed that the sev-

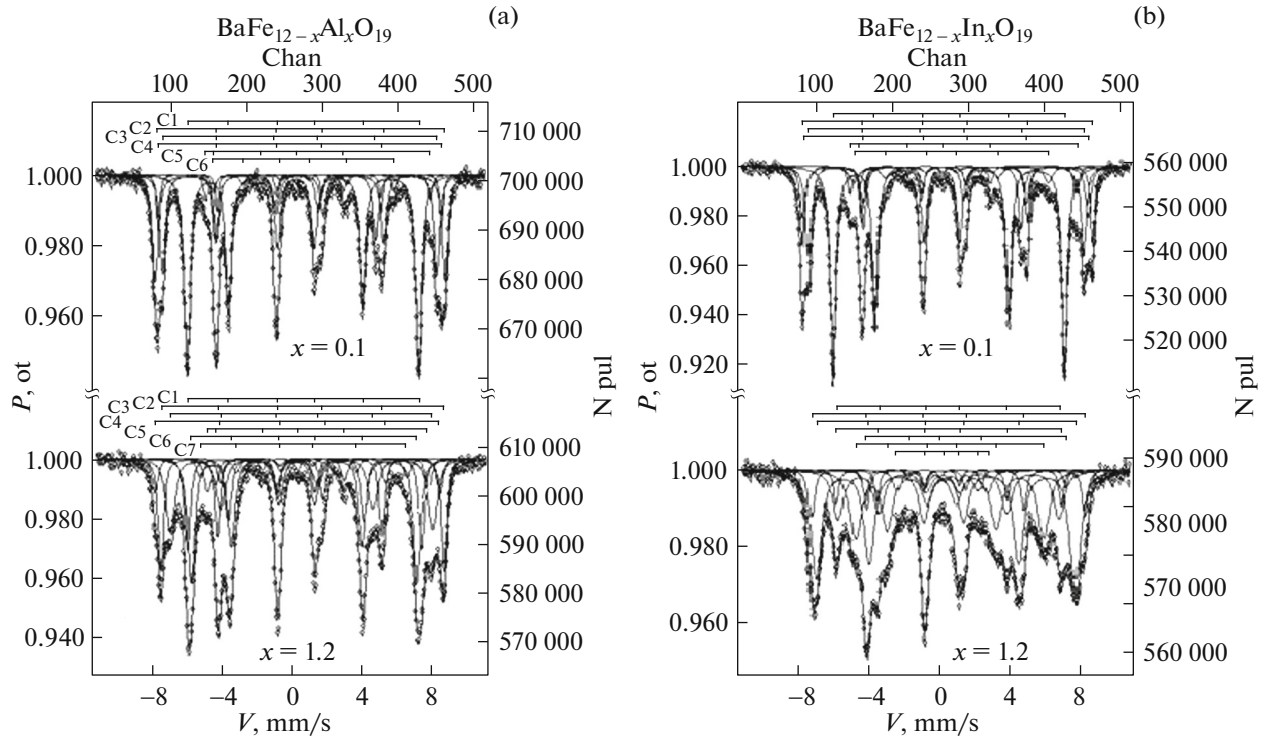

Fig. 3. Mössbauer spectroscopy data for (a) the $BaFe_{12-x}Al_xO_{19}$ and (b) $BaFe_{12-x}In_xO_{19}$, where $x = 0.1$ and 1.2.

enth sextet can be referred to the formation of a new nonequivalent position $12k^2$ (this is also a distorted nonequivalent sublattice $12k$ with a different binding energy). This is a quite complex case for the unambiguous interpretation of the cation distribution, but we can most likely propose the following explanation. We believe that diamagnetic ions in the Al-substituted samples ($x = 1.2$) occupy the $2b$ and $12k$ positions, which leads to an attenuation and even breaking of the exchange couplings Fe^{3+} ($2b$)–O–Fe^{3+} ($12k$) and Fe^{3+} ($2a$)–O–Fe^{3+} ($12k$).

The effective magnetic fields at ^{57}Fe nuclei in $BaFe_{10.8}Al_{1.2}O_{19}$ have the following order: $B_{eff}Fe(2a) > B_{eff}Fe(4f_2) > B_{eff}Fe(4f_1) > B_{eff}Fe(12k) > B_{eff}Fe(12k^1) > B_{eff}Fe(2b) > B_{eff}Fe(12k^2)$. For the In-substituted sample ($x = 1.2$) we believe that diamagnetic ions predominantly occupy $2b$ and $2a$ positions and weaken the order of exchange couplings in the bond Fe + ($2b$)–O–Fe^{3+}($12k$) and Fe + ($2b$)–O–Fe^{3+}($2a$). Fields on ^{57}Fe nuclei $BaFe_{10.8}In_{1.2}O_{19}$ are arranged in the following order: $B_{eff}Fe(4f_2) > B_{eff}Fe(4f_1) > B_{eff}Fe(2a) > B_{eff}Fe(12k) > B_{eff}Fe(2b) > B_{eff}Fe(12k^1) > B_{eff}Fe(12k^2)$.

Figure 4 shows the theoretical data calculated according to Eq. (2). To calculate the anisotropy field, we used the data for the spherical shape of the crystallites in an approximation of low size dispersion. The data shown in Fig. 5 confirm the statement that ions with different electronic structures differently influence the electrophysical properties (the NFMR resonant frequency shift). From Fig. 5, it can be seen that the increase in the NFMR resonant frequency (due to the increase in the magnetocrystalline anisotropy (MCA)) is only characteristic of the case with the Al^{3+} substitution. Other ions induce a decrease in the resonant frequency (f_{res}). The MCA value for the nonsubstituted barium hexaferrite $BaFe_{12}O_{19}$ is 16–17 kOe.

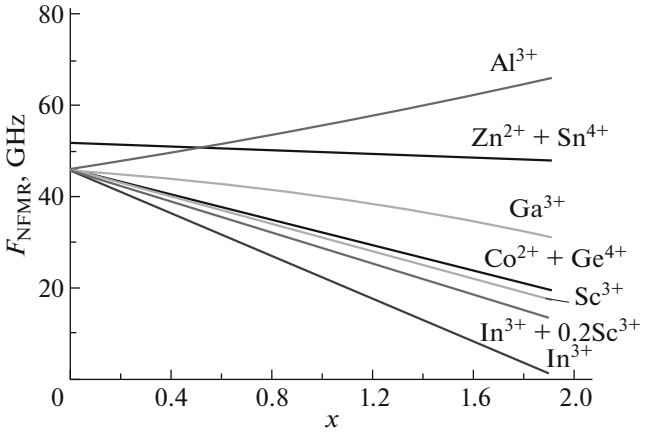

Fig. 4. Theoretical concentration dependences of the NFMR frequency for barium hexaferrites substituted with various ions.

Table 1. Parameters of the Mössbauer spectroscopy for the $BaFe_{12-x}Al_xO_{19}$ and $BaFe_{12-x}In_xO_{19}$ ($x = 0.1$ and $x = 1.2$) samples

Sample	Spectrum component	Isomer shift δ, mm/s	Quadrupole splitting Δ, mm/s	Magnetic fields B, T	Area components S, %
Nonsubstituted barium hexaferrite					
$BaFe_{12}O_{19}$	C1–12k(Fe^{3+})$_{VI}$	0.36	0.41	41.2	50.4
	C2–4f_2(Fe^{3+})$_{VI}$	0.37	0.17	51.6	19.2
	C3–4f_1(Fe^{3+})$_{IV}$	0.27	0.2	49.0	18.3
	C4–2s(Fe^{3+})$_{VI}$	0.33	0	50.5	7
	C5–2b(Fe^{3+})$_{V}$	0.29	2.21	40.1	5.1
Al-substituted barium hexaferrite					
$BaFe_{11.9}Al_{0.1}O_{19}$ $x = 0.1$	C1–12k(Fe^{3+})$_{VI}$	0.35	0.41	41.3	45.9
	C2–4f_2(Fe^{3+})$_{VI}$	0.38	0.18	51.4	15.8
	C3–4f_1(Fe^{3+})$_{IV}$	0.27	0.21	48.9	23
	C4–2a(Fe^{3+})$_{VI}$	0.35	0.03	50.6	5.5
	C5–2b(Fe^{3+})$_{IV}$	0.29	2.16	40.0	5.9
	C6–12k(Fe^{3+})$_{V}$	**0.29**	**0.36**	**39.8**	**3.9**
$BaFe_{10.8}Al_{1.2}O_{19}$ $x = 1.2$	C1–12k(Fe^{3+})$_{VI}$	0.34	0.47	41.5	16.5
	C2–4f_2(Fe^{3+})$_{VI}$	0.39	0.16	50.3	19.3
	C3–4f_1(Fe^{3+})$_{IV}$	0.27	0.26	46.6	20.3
	C4–2a(Fe^{3+})$_{VI}$	0.33	−0.32	50.6	6.3
	C5–2b(Fe^{3+})$_{IV}$	0.26	2.15	38.3	6
	C6–12k^1(Fe^{3+})$_{V}$	**0.34**	**0.42**	**40.0**	**27.6**
	C7–12k"(Fe^{3+})$_{VI}$	**0.32**	**0.43**	**36.7**	**4**
In-substituted barium hexaferrite					
$BaFe_{11.9}In_{0.1}O_{19}$ $x = 0.1$	C1–12k(Fe^{3+})$_{VI}$	0.35	0.41	41.1	46.0
	C2–4f_2(Fe^{3+})$_{VI}$	0.38	0.18	51.3	16.3
	C3–4f_1(Fe^{3+})$_{IV}$	0.27	0.19	48.7	22.4
	C4–2a(Fe^{3+})$_{VI}$	0.35	0.03	50.4	5.0
	C5–2b(Fe^{3+})$_{IV}$	0.26	2.16	40.1	4.6
	C6–12k'(Fe^{3+})$_{V}$	**0.38**	**0.51**	**34.5**	**5.7**
$BaFe_{10.8}In_{1.2}O_{19}$ $x = 1.2$	C1–12k(Fe^{3+})$_{VI}$	0.34	0.38	39.1	16.1
	C2–4f_2(Fe^{3+})$_{VI}$	0.40	0.11	48.3	14.6
	C3–4f_1(Fe^{3+})$_{IV}$	0.30	0.10	45.9	28.8
	C4–2a(Fe^{3+})$_{VI}$	0.35	0.32	40.4	9.4
	C5–2b(Fe^{3+})$_{IV}$	0.28	2.31	36.0	3.7
	C6–12k^1(Fe^{3+})$_{V}$	**0.34**	**0.41**	**33.5**	**20.6**
	C7–12k"(Fe^{3+})$_{VI}$	**0.41**	**–0.48**	**16.4**	**6.8**

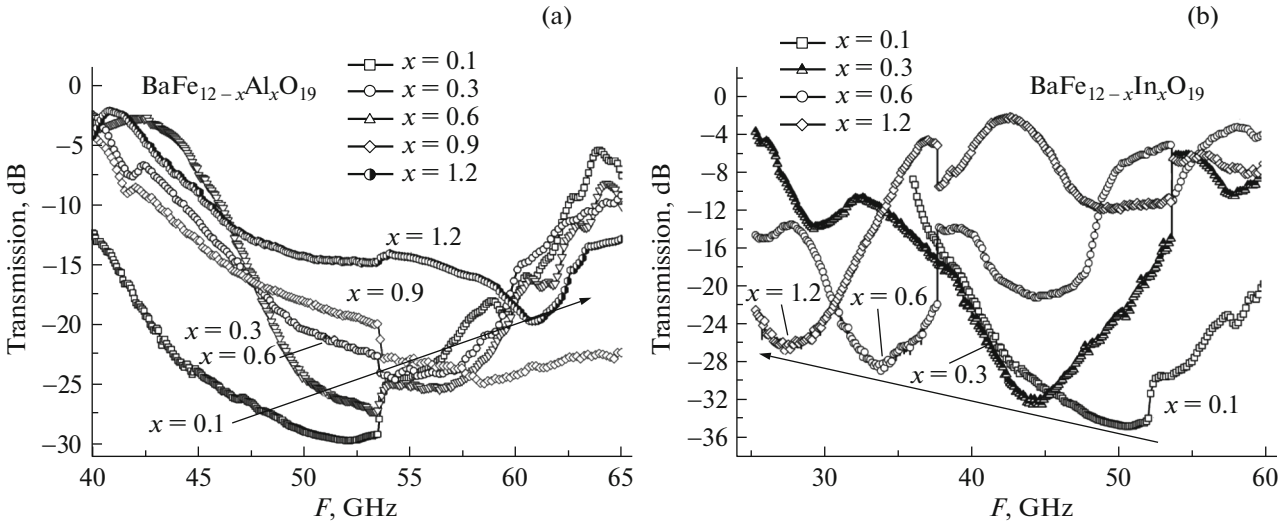

Fig. 5. Frequency dependences of the transmission coefficient for the samples with various concentrations of (a) Al^{3+} and (b) In^{3+} cations, where $0.1 \le x \le 1.2$.

The resonant frequency peak was observed at 49–50 GHz. In $BaFe_{12-x}Al_xO_{19}$, the substitution of aluminum ions for iron ions induces the increase in MCA from 16–17 kOe ($x = 0$) to 23 kOe ($x = 1.2$). This fact can be explained by the attenuation of the interlattice exchange Fe^{3+}–O^{2-}–Fe^{3+} interaction due to the magnetic structure frustration. According to the Mössbauer spectroscopy data, the attenuation will be preferentially noted for the interactions of positions 2*b*, 2*a*, and 12*k* (the attenuation of the long range order of the exchange interactions of the Fe^{3+} (2*b*)–O–Fe^{3+} (12*k*) coupling). In the dependence on the aluminum ion concentration, we will be observe the competition of the attenuations of the bonds between Fe^{3+} (2*b*)–O–Fe^{3+} (2*a*) (at $x \le 0.6$) and Fe^{3+} (2*a*)–O–Fe^{3+} (12*k*) (at $0.6 < x \le 1.2$). In $BaFe_{12-x}In_xO_{19}$, the substitution of In^{3+} ions for iron ions leads to the decrease in the MCA value from 16–17 kOe ($x = 0$) to 10–11 kOe ($x = 1.2$). This result is also can be explained by the attenuation of the interlattice exchange Fe^{3+}–O^{2-}–Fe^{3+} interaction due to the magnetic structure frustration. However, the features of the intersublattice interaction should be analyzed for explaining the microwave characteristics in the context of analyzing the electronic structure of the diamagnetic ions and the influence of the crystal field energy.

Figure 5 shows the spectra of the EMR transmission through the samples with different concentrations of Al^{3+} (Fig. 5a) and In^{3+} (Fig. 5b) cations. Figure 6 shows the concentration dependences of the amplitude–frequency characteristics of the electromagnetic properties of the barium hexaferrite substituted with Al^{3+} (Fig. 6a) and In^{3+} (Fig. 6b) ions.

The most intense decrease in the transmission is observed in the frequency range 20–65 GHz in all the samples, because of the absorption processes caused by the NFMR phenomenon. The abscissa of the global minimum of the EMR transmission spectrum determines the resonance frequency (f_{res}). The ordinate of the global minimum of the EMR transmission spectrum determines the resonance amplitude (A_{res}) of the absorption process.

The Al-substituted $BaFe_{12-x}D_xO_{19}$ samples demonstrated the increase in f_{res} with the Al^{3+} ion concentration. The resonance frequency peak (f_{res}) shifted from 51 to 61 GHz in the concentration range from $x = 0.1$ to $x = 1.2$, respectively (Fig. 6b). The results agreed well with the theoretical data obtained by numerical calculations using Eq. (2).

Thus, the increase in the Al^{3+} ion concentration leads to the decrease in the amplitude (A_{res}) from −29.5 to −20 dB (Fig. 6a). The In-substituted $BaFe_{12-x}D_xO_{19}$ samples demonstrated the decrease in f_{res} as the In^{3+} ion concentration increased. The resonance frequency peak (f_{res}) shifted from 50.5 to 27 GHz in the concentration range from $x = 0.1$ to $x = 1.2$, respectively (Fig. 6d). The results agreed well with the theoretical data. Some deviation from the linear dependences in the frequency dependences for concentrations $x \ge 0.9$ can be due to internal microstress (microstrain in the crystallites because of the large In^{3+} ionic radius). Amplitude A_{res} decreased from −34.9 to −26.9 dB in the same concentration range, respectively (Fig. 6c).

Figure 7 demonstrates the influence of an external magnetic field on the amplitude–frequency characteristics of the samples.

It was noted above that the applying of the energy of an external magnetic field can lead to an increase in

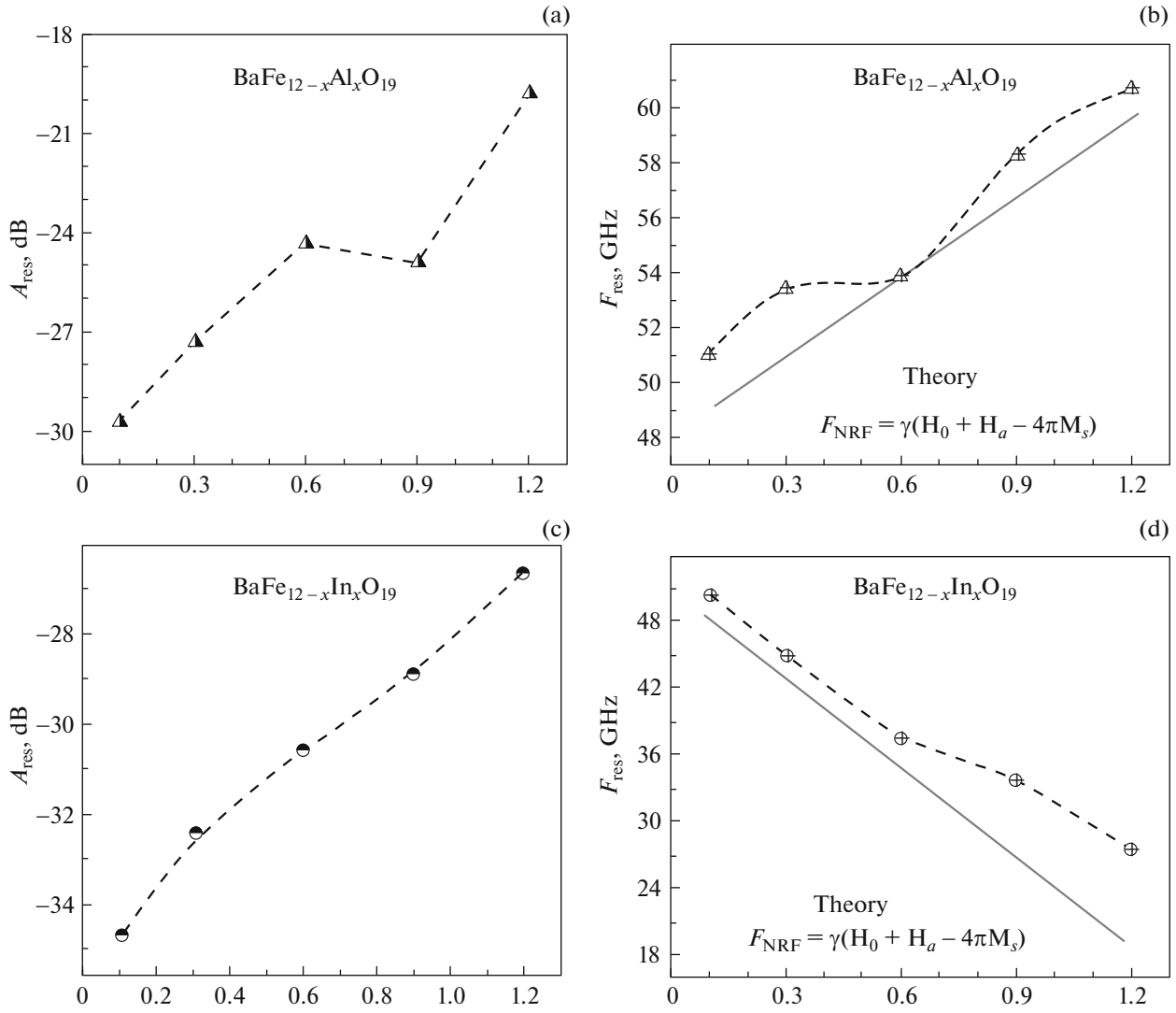

Fig. 6. Concentration dependences of the resonance amplitude (A_{res}) and resonance frequency (f_{res}) for solid solutions of (a, b) Al^{3+}-substituted and (c, d) In^{3+}-substituted barium hexaferrite in the concentration range $0.1 \le x \le 1.2$.

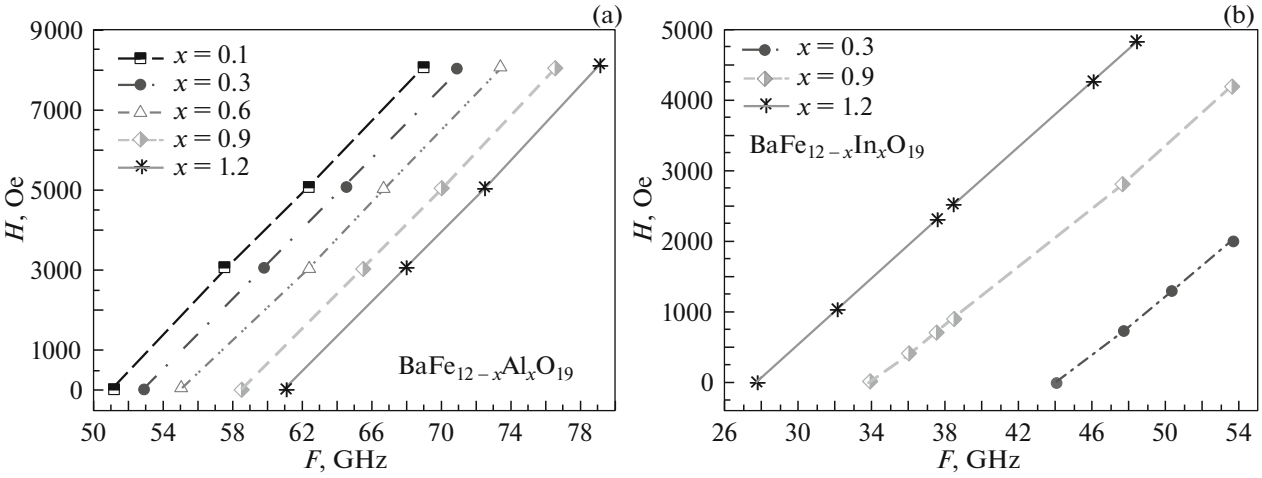

Fig. 7. Dependences of the NFMR resonance frequency on external magnetic field for solid solutions of (a, b) Al^{3+}-substituted and (c, d) In^{3+}-substituted barium hexaferrite in the concentration range $0.1 < x < 1.2$.

MCA and, correspondingly, shift the NFMR frequency to higher frequencies. The studies of the solid solutions $BaFe_{12-x}Al_xO_{19}$ (Fig. 7a) and $BaFe_{12-x}In_xO_{19}$ (Fig. 7b) showed a nearly linear shift of the resonance frequency (f_{res}) to higher frequencies. The energy of an external magnetic field increases the intensity of the intrasublattice exchange interactions, which increases the resonance frequency of the spin precession. The possibility of controlling the amplitude-frequency characteristics not only by varying the chemical composition, but also by external magnetic fields, opens serious perspectives of applying these materials in practice.

When searching for materials that effectively work in the microwave range, the region caused by NFMR is of the greatest interest. Ferromagnetic resonance leads to the loss of the electromagnetic field energy that are a result of a number of processes during cation spin precession for ferro- or ferrimagnetics related to additional fluctuations of the crystal lattice sites. The spin precession during NFMR occurs under influence of internal local magnetic fields as a result of the intrinsic magnetic anisotropy. The magnetization vector precesses around the easy-magnetization axis. The physical principles responsible for the NFMR loss are the same as those during the induced ferromagnetic resonance. They are additional fluctuations of hexaferrite crystal lattice portions due to spin waves. The interaction of spin waves with the crystal lattice leads the conversion of a part of the external field energy exciting the thermal spin precession and, therefore, spin waves to thermal lattice fluctuations. In this case, the NFMR frequency is determined by the energy of the magnetization vector rotation in the easy-magnetization plane and also the energy of rotation from this plane.

4. CONCLUSIONS

The main purpose of this work was to study the correlation of the chemical composition, the structure, and the microwave characteristics of solid solutions of the $BaFe_{12-x}D_xO_{19}$ ($0.1 \le x \le 1.2$) barium hexaferrite substituted with diamagnetic Al^{3+} and In^{3+} ions. To do this, it was necessary to perform precise studies by the powder diffraction method, the Mössbauer spectroscopy, and the high-frequency measurements of the transmittances. The powder diffraction data showed that the dependence of the unit cell parameters on the concentration is closely related to the effective ionic radii of the substituting ions (0.540 Å for Al^{3+} and 0.940 Å for In^{3+}). The character of the distribution of the diamagnetic ions was determined by the Mössbauer spectroscopy. It is shown that the distributions of the diamagnetic ions in low concentration ($x < 0.3$) are similar for the Al- and In-substituted compositions. However, the distributions of the Al- and In-substituting ions in corresponding compositions become different as their concentrations increase This circumstance variously influences the attenuation of the intersublattice exchange interactions in the Fe^{3+}–O^{2-}–Fe^{3+} chains due to various mechanisms of the magnetic structure frustration. It is shown that the concentration substitution level and the nature of the substituting ions variously influence the amplitude–frequency characteristics of the solid solutions of the $BaFe_{12-x}D_xO_{19}$ ($0.1 \le x \le 1.2$) barium hexaferrite substituted with diamagnetic Al^{3+} and In^{3+} ions. The EMR energy loss during the interaction with the study samples are provided by the absorption processes due to the natural ferromagnetic resonance. These processes are based on a change in the chemical composition. The Al-substituted compositions demonstrate nearly linear increase in the resonance frequency (f_{res}) as the resonance amplitude (A_{res}) decreases. Conversely, the In-substituted samples demonstrate a sharp decrease in the resonance frequency, which is due to the appearance of internal microstresses and microdeformations. The anisotropy change was explained by the attenuation of the intensity of the intersublattice superexchange interactions. It is shown that the external magnetic field energy almost linearly shifts the resonance frequency to higher frequencies, which is explained by an additional contribution to the MCA increase.

The results of the studies of the microwave characteristics in the frequency range 20–65 GHz are of great interest from the practical point of view due to a possibility of controlling the electrodynamic characteristics by a change in the chemical composition of the hexagonal ferrite and also by applying an external magnetic field.

ACKNOWLEDGMENTS

The authors are grateful to A.M. Balagurov for the help in the interpretation of the experimental data.

This work was supported by Belarussian Republican Foundation for Basic Research, project no. F17D-003.

REFERENCES

1. V. Adelskold, Avk. Miner. A **1**, 12 (1938).
2. S. V. Trukhanov, A. V. Trukhanov, V. G. Kostishyn, and L. V. Panina, Dalton Trans. **46**, 9010 (2017).
3. O. P. Aleshko-Ozhevskii, R. A. Sizov, I. I. Yamzin, and V. A. Lubimtsev, Sov. Phys. JETP **28**, 425 (1969).
4. L. Wang, H. Yu, X. Ren, and G. Xu, J. Alloys Compd. **588**, 212 (2014).
5. P. Meng, K. Xiong, L. Wang, S. Li, Y. Cheng, and G. Xu, J. Alloys Compd. **628**, 75 (2015).
6. V. A. Turchenko, A. V. Trukhanov, I. A. Bobrikov, S. V. Trukhanov, and A. M. Balagurov, Crystallogr. Rep. **60**, 629 (2015).
7. A. V. Trukhanov, L. V. Panina, S. V. Trukhanov, V. A. Turchenko, and M. Salem, Chin. Phys., B **25**, 016102 (2016).

8. D. A. Vinnik, D. A. Zherebtsov, L. S. Mashkovtseva, S. Nemrava, M. Bischoff, N. S. Perov, A. S. Semisalova, I. V. Krivtsov, L. I. Isaenko, G. G. Mikhailov, and R. Niewa, J. Alloys Compd. **615**, 1043 (2014).
9. A. M. Y. El-Lawindy, S. A. Mansour, M. Hafiz, H. H. Hassan, and A. A. Ali, Int. J. Appl. Ceram. Technol. **7**, 868 (2010).
10. X. Liu, J. Wang, L. M. Gan, S. C. Ng, and J. Ding, J. Magn. Magn. Mater. **184**, 344 (1998).
11. E. Richter, T. J. E. Miller, T. W. Neumann, and T. L. Hudson, IEEE Trans. Ind. Appl. **1A-21**, 644 (1985).
12. Q. A. Pankhurst and R. S. Pollard, J. Phys.: Condens. Mater. **5**, 8487 (1993).
13. Y. Tokunaga, Y. Kaneko, D. Okuyama, S. Ishiwata, T. Arima, S. Wakimoto, K. Kakurai, Y. Taguchi, and Y. Tokura, Phys. Rev. Lett. **105**, 257201 (2010).
14. B. Warcholinski, A. Gilewicz, T. A. Kuznetsova, T. I. Zubar, S. A. Chizhik, S. O. Abetkovskaia, and V. A. Lapitskaya, Surf. Coat. Technol. **117**, 319 (2017).
15. E. V. Sadyrin, B. I. Mitrin, S. M. Aizikovich, and T. I. Zubar, Mater. Phys. Mech. **28**, 1 (2016).
16. G. Tan and X. Chen, J. Magn. Magn. Mater. **327**, 87 (2013).
17. A. V. Trukhanov, V. O. Turchenko, I. A. Bobrikov, S. V. Trukhanov, I. S. Kazakevich, and A. M. Balagurov, J. Magn. Magn. Mater. **253**, 393 (2015).
18. A. V. Trukhanov, S. V. Trukhanov, L. V. Panina, V. G. Kostishyn, D. N. Chitanov, I. S. Kazakevich, An. V. Trukhanov, V. A. Turchenko, and M. Salem, Ceram. Int. **43**, 5635 (2017).
19. S. V. Trukhanov, A. V. Trukhanov, V. G. Kostishin, L. V. Panina, I. S. Kazakevich, V. A. Turchenko, and V. V. Kochervinskiy, JETP Lett. **103**, 100 (2016).
20. A. V. Trukhanov, S. V. Trukhanov, V. G. Kostishin, L. V. Panina, M. M. Salem, I. S. Kazakevich, V. A. Turchenko, V. V. Kochervinskii, and D. A. Krivchenya, Phys. Solid State **59**, 737 (2017).
21. L. Li, K. Chen, H. Liu, G. Tong, H. Qian, and B. Hao, J. Alloys Compd. **11**, 557 (2013).
22. N. Velhal, G. Kulkarni, D. Mahadik, P. Chowdhury, H. Barshilia, and V. Puri, J. Alloys Compd. **682**, 730 (2016).
23. L. I. Krenev, E. V. Sadyrin, S. M. Aizikovich, and T. I. Zubar, Springer Proc. Phys. **193**, 184 (2017).
24. B. Warcholinski, A. Gilewicz, O. Lupicka, A. S. Kuprin, G. N. Tolmachova, V. D. Ovcharenko, I. V. Kolodiy, M. Sawczak, A. E. Kochmanska, P. Kochmanski, T. A. Kuznetsova, T. I. Zubar, A. L. Khudoley, and S. A. Chizhik, Surf. Coat. Technol. **920**, 309 (2016).
25. F. A. Miranda, F. W. van Keuls, and R. R. Romanofsky, IEEE Trans. Microwave Theory Technol. **48**, 1181 (2000).
26. J.-S. Kim, Y.-H. Lee, B. Lee, J.-C. Lee, J. J. Choi, and J. Y. Kim, J. Electr. Eng. Technol. **9**, 273 (2014).
27. L. Vovchenko, L. Matzui, O. Brusylovets, V. Oliynyk, V. Launets, A. Shames, O. Yakovenko, and N. Skoryk, Mat.-wiss. Werkstofftech. **47**, 139 (2016).
28. D. Chen, Y. Liu, Y. Li, K. Yang, and H. Zhang, J. Magn. Magn. Mater. **37–38**, 65 (2013).
29. T. Kuznetsova, T. Zubar, S. Chizhik, A. Gilewicz, O. Lupicka, and B. Warcholinski, J. Mater. Eng. Perform. **25**, 5450 (2016).
30. V. Zavaleyev, J. Walkowicz, T. Kuznetsova, and T. Zubar, Thin Solid Films **153**, 638 (2017).
31. D. A. Vinnik, A. B. Ustinov, D. A. Zherebtsov, V. V. Vitko, S. A. Gudkova, I. Zakharchuk, E. Lähderanta, and R. Niewa, Ceram. Int. **41**, 12728 (2015).
32. S. V. Trukhanov, A. V. Trukhanov, V. O. Turchenko, V. G. Kostishin, L. V. Panina, I. S. Kazakevich, and A. M. Balagurov, J. Magn. Magn. Mater. **417**, 130 (2016).
33. S. V. Trukhanov, A. V. Trukhanov, V. G. Kostishyn, L. V. Panina, An. V. Trukhanov, V. A. Turchenko, D. I. Tishkevich, E. L. Trukhanova, V. V. Oleynik, O. S. Yakovenko, L. Yu. Matzui, and D. A. Vinnik, J. Magn. Magn. Mater. **442**, 300 (2017).
34. T. A. Kuznetsova, T. I. Zubar, V. A. Lapitskaya, K. A. Sudzilouskaya, S. A. Chizhik, A. L. Didenko, V. M. Svetlichnyi, M. E. Vylegzhanina, V. V. Kudryavtsev, and T. E. Sukhanova, IOP Conf. Ser. Mater. Sci. Eng. **256**, 1 (2017).
35. S. Kuprin, T. A. Kuznetsova, A. Gilewicz, G. N. Tolmachova, V. D. Ovcharenko, S. O. Abetkovskaia, T. I. Zubar, A. L. Khudoley, S. A. Chizhik, O. Lupicka, and B. Warcholinski, Probl. At. Sci. Technol. **6106**, 147 (2016).
36. A. V. Trukhanov, S. V. Trukhanov, L. V. Panina, V. G. Kostishyn, I. S. Kazakevich, An. V. Trukhanov, E. L. Trukhanova, V. O. Natarov, V. A. Turchenko, M. M. Salem, and A. M. Balagurov, J. Magn. Magn. Mater. **426**, 487 (2017).
37. S. V. Trukhanov, A. V. Trukhanov, V. A. Turchenko, An. V. Trukhanov, E. L. Trukhanova, D. I. Tishkevich, V. M. Ivanov, T. I. Zubar, M. Salem, V. G. Kostishyn, L. V. Panina, D. A. Vinnik, and S. A. Gudkova, Ceram. Int. **44**, 290 (2018).
38. H. M. Rietveld, J. Appl. Crystallogr. **2**, 65 (1969).
39. http://www.ill.eu/sites/fullprof/.

Translated by Yu. Ryzhkov